Arabidopsis Type I Proton-Pumping Pyrophosphatase Expresses Strongly in Phloem, Where It Is Required for Pyrophosphate Metabolism and Photosynthate Partitioning[1][OPEN]

Gaston A. Pizzio[2], Julio Paez-Valencia[2], Aswad S. Khadilkar[2], Kamesh Regmi, Araceli Patron-Soberano, Shangji Zhang, Jonathan Sanchez-Lares, Tara Furstenau, Jisheng Li, Concepcion Sanchez-Gomez, Pedro Valencia-Mayoral, Umesh P. Yadav, Brian G. Ayre, and Roberto A. Gaxiola*

School of Life Sciences, Arizona State University, Tempe, Arizona 852872 (G.A.P., J.P.-V., K.R., S.Z., J.S.-L., T.F., J.L., R.A.G.); Department of Botany, University of Wisconsin, Madison, Wisconsin 53706 (J.P.-V.); Department of Biological Sciences, University of North Texas, Denton, Texas 762031 (A.S.K., U.P.Y., B.G.A.); División de Biología Molecular, Laboratorio Nacional de Investigaciones en Nanociencias y Nanotecnología Instituto Potosino de Investigación Científica y Tecnológica, A.C. 78216 San Luis Potosí, Mexico (A.P.-S.); and Departamento de Patología, Hospital Infantil de México, Federico Gómez, Mexico (C.S.-G., P.V.-M.)

Phloem loading is a critical process in plant physiology. The potential of regulating the translocation of photoassimilates from source to sink tissues represents an opportunity to increase crop yield. Pyrophosphate homeostasis is crucial for normal phloem function in apoplasmic loaders. The involvement of Arabidopsis (*Arabidopsis thaliana*) type I proton-pumping pyrophosphatase (AVP1) in phloem loading was analyzed at genetic, histochemical, and physiological levels. A transcriptional *AVP1* promoter::GUS fusion revealed phloem activity in source leaves. Ubiquitous *AVP1* overexpression (*35S*::*AVP1* cassette) enhanced shoot biomass, photoassimilate production and transport, rhizosphere acidification, and expression of sugar-induced root ion transporter genes (*POTASSIUM TRANSPORTER2* [*KUP2*], *NITRATE TRANSPORTER2.1* [*NRT2.1*], *NRT2.4*, and *PHOSPHATE TRANSPORTER1.4* [*PHT1.4*]). Phloem-specific *AVP1* overexpression (*Commelina Yellow Mottle Virus promoter* [*pCOYMV*]::*AVP1*) elicited similar phenotypes. By contrast, phloem-specific *AVP1* knockdown (*pCoYMV*::$_{RNAi}$*AVP1*) resulted in stunted seedlings in sucrose-deprived medium. We also present a promoter mutant *avp1-2* (SALK046492) with a 70% reduction of expression that did not show severe growth impairment. Interestingly, AVP1 protein in this mutant is prominent in the phloem. Moreover, expression of an *Escherichia coli*-soluble pyrophosphatase in the phloem (*pCoYMV*::*pyrophosphatase*) of *avp1-2* plants resulted in severe dwarf phenotype and abnormal leaf morphology. We conclude that the Proton-Pumping Pyrophosphatase AVP1 localized at the plasma membrane of the sieve element-companion cell complexes functions as a synthase, and that this activity is critical for the maintenance of pyrophosphate homeostasis required for phloem function.

The partitioning of photoassimilates between their sites of production and their sites of utilization in harvestable regions is a major determinant of crop yield (Giaquinta et al., 1983; Braun et al., 2014; Ruan, 2014), and the potential of regulating this translocation promises substantial opportunities for yield increases. Photosynthates produced in mature, fully developed source leaves are distributed by the phloem to support growth and development of sinks. The phloem in fully developed source leaves collects photosynthates from the mesophyll and initiates a mass flow of reduced carbon within the phloem sieve elements (Rennie and Turgeon, 2009).

Phloem loading of Suc into the sieve element-companion cell (SE-CC) complex of plants that load from the apoplasm requires the active uptake of Suc from the extracellular space by Suc/proton symporters (Giaquinta et al., 1983; Gottwald et al., 2000; Ayre, 2011). This process is energized by the proton motive force (PMF) established by plasma membrane (PM) P-type H^+-adenosine triphosphatases (ATPases). To generate the required ATP, a portion of the loaded Suc is oxidized in companion cells. Particularly, in these cells, Suc oxidation through the pyrophosphate (PP_i)-dependent Suc Synthase pathway is essential (Ruan, 2014), but how this PP_i supply is maintained remains obscure.

The first indication for this PP_i dependency in companion cells came from the ectopic expression of the *Escherichia coli* soluble pyrophosphatase (ppa) driven by the cauliflower mosaic virus (CaMV) *35S* promoter in tobacco (*Nicotiana tabacum*) and potato (*Solanum*

[1] This work was supported by the National Science Foundation (grant nos. IOS–1122148 to G.A.P., J.P.-V., K.R., and R.A.G. and IOS–1121819 to A.S.K., U.P.Y., and B.G.A.).

[2] These authors contributed equally to the article.

* Address correspondence to roberto.gaxiola@asu.edu.

The author responsible for distribution of materials integral to the findings presented in this article in accordance with the policy described in the Instructions for Authors (www.plantphysiol.org) is: Roberto A. Gaxiola (roberto.gaxiola@asu.edu).

[OPEN] Articles can be viewed without a subscription.
www.plantphysiol.org/cgi/doi/10.1104/pp.114.254342

tuberosum) plants (Jelitto et al., 1992; Sonnewald, 1992). These plants showed increased levels of soluble sugars in source leaves, but this enhanced sugar content did not result in higher shoot and root biomass (Jelitto et al., 1992). On the contrary, *35S:ppa* tobacco and potato plants showed stunted growth, reduced root formation, and early necrosis in mature leaves. It was, thus, suggested that the stunted growth observed in these plants resulted from the removal of PP_i in the phloem and a block to Suc oxidation (Jelitto et al., 1992; Sonnewald, 1992). Lerchl et al. (1995) confirmed this hypothesis by the phloem-specific expression of the *E. coli* ppa in tobacco and showed that removal of cytosolic PP_i from companion cells triggered the same phenotype observed in the *35S:ppa* plants. Of note, Lerchl et al. (1995) showed that phloem-specific expression of a yeast (*Saccharomyces cerevisiae*) invertase restored wild-type phenotypes by allowing Suc to enter glycolysis through a Suc synthase- and PP_i-independent pathway, emphasizing the relevance of PP_i in phloem loading.

Type I Proton-Pumping Pyrophosphatases (H^+-PPases) are transmembrane proteins participating in control of PP_i homeostasis. In plants, these were originally described as PP_i-driven vacuolar proton pumps that contribute to the PMF across the tonoplast (Rea et al., 1992). However, in vivo data obtained with the H^+-PPase from the proteobacterium *Rhodospirillum rubrum* were consistent with the capacity of this enzyme to play two distinct roles depending on location and conditions. It can act as an intracellular H^+ pump in the acidocalcisomes (Seufferheld et al., 2004) or a PP_i synthase in the chromatophore membranes during illumination (Baltscheffsky et al., 1966). Bacterial H^+-PPases share significant homology with their plant counterparts (Seufferheld et al., 2011). Furthermore, Rocha Facanha and de Meis (1998) presented in vitro evidence with tonoplast fractions of maize (*Zea mays*) coleoptiles and seeds consistent with the PP_i synthase function of the H^+-PPase. Rocha Facanha and de Meis (1998) suggested that, given the appropriate thermodynamic conditions in vivo, the H^+-PPase could operate as a system of energy conservation with a role in the maintenance of cytosolic PP_i levels. Additional data confirming the reversibility of the pump came from experiments in vacuoles from oranges (*Citrus sinensis*; Marsh et al., 2000).

Interestingly, double-labeling immunolocalizations showed the H^+-PPase and the well-characterized P-type H^+-ATPase in proximity at the PM of companion cells in *Ricinus communis* (Langhans et al., 2001). Langhans et al. (2001) suggested that both H^+ pumps generate the PMF to maintain high Suc, K^+, and amino acid concentrations in the phloem. Coimmunogold labeling studies also showed that Arabidopsis (*Arabidopsis thaliana*) type I proton-pumping pyrophosphatase (AVP1) is localized at the PM of SE-CC complexes (Paez-Valencia et al., 2011). However, the proposition that H^+-PPases contribute to the PMF across the PM in the phloem was challenged on thermodynamic grounds, because the free energy of hydrolysis of PP_i is lower than that of ATP and insufficient to drive a proton out against the prevailing electrochemical gradient at this interface (Davies, 1997).

Initial studies found that overexpression of *AVP1* in Arabidopsis resulted in enhanced salt tolerance and drought resistance (Gaxiola et al., 2001). The salt-tolerant phenotype was explained by an increased capacity of Na^+ uptake into vacuoles, and the drought-resistance phenotype was attributed to an enhanced vacuolar osmoregulatory capacity (Gaxiola et al., 2001, 2002). Moreover, a study on the variation of salinity tolerance in Arabidopsis ecotypes reported a positive relationship between salt tolerance and *AVP1* expression (Jha et al., 2010). In the last decade, overexpression of genes encoding H^+-PPases was successful in increasing salt and drought resistance in 14 different crops (e.g. alfalfa [*Medicago sativa*], barley [*Hordeum vulgare*], cotton [*Gossypium hirsutum*], maize, and rice [*Oryza sativa*] among others; Bao et al., 2008; Li et al., 2008; Pasapula et al., 2011; Schilling et al., 2014; Yang et al., 2014; R.A. Gaxiola, G.A. Pizzio, and K. Regmi, unpublished data). In addition to salt and drought tolerance, increased shoot and root biomass and yield, enhanced root acidification, and improved nutrient use efficiencies were also reported (Yang et al., 2007, 2014; Lv et al., 2008; Pasapula et al., 2011; Pei et al., 2012; Arif et al., 2013; Paez-Valencia et al., 2013; Li et al., 2014; Schilling et al., 2014; Wang et al., 2014). These phenotypes are not well explained by the traditional model of type I H^+-PPases operating solely on the vacuole to energize the tonoplast (Martinoia et al., 2007).

Given the localization of H^+-PPases at the PM of SE-CC complexes (Langhans et al., 2001; Paez-Valencia et al., 2011), the reversibility of the plant enzyme (Rocha Facanha and de Meis, 1998; Marsh et al., 2000), the thermodynamic constraints of PP_i hydrolysis coupled to proton transport (Davies, 1997), and the key role of PP_i in companion cells (Lerchl et al., 1995), a model was recently proposed (Gaxiola et al., 2012), in which the PM-localized H^+-PPase can function as a synthase in the phloem to maintain PP_i homeostasis for the Suc oxidation and ATP production required for the generation of the PMF through PM H^+-ATPase activity. As a corollary, increased PP_i synthase activity in companion cells would augment phloem loading and long-distance transport in transgenic plants by indirectly energizing the SE-CC complex of source leaves.

In this work, we performed genetic, histochemical, and physiological experiments to test the above model. An *AVP1* promoter *β-glucuronidase* (*uidA*; encoding GUS) chimera showed conspicuous phloem activity. Ubiquitous and phloem-specific *AVP1* overexpression enhanced shoot biomass and photoassimilate production and transport. In addition, phloem-specific *AVP1* knockdown resulted in stunted growth in both shoot and roots. A promoter mutant, *avp1-2*, with a significant reduction of *AVP1* expression did not show severe growth impairment. Phloem expression of a soluble ppa in *avp1-2* plants resulted in severe dwarf phenotype. We conclude that AVP1 and PP_i homeostasis are essential to support phloem function and growth in Arabidopsis.

RESULTS

A 1.7-kb *AVP1* Promoter GUS Reporter Reveals Vascular Expression in Columbia-0 Arabidopsis Seedlings and Adult Plants

In situ hybridization showed that the *AVP1* gene is transcribed in Columbia-0 (Col-0) Arabidopsis seedlings in all shoot meristems as well as the endodermal/pericycle ring of mature roots, developing leaves, sepals, petals, stamens, and carpels (Li et al., 2005). Here, we used transgenic plants carrying the 1.7-kb *AVP1* promoter (Yang et al., 2007) fused to the open reading frame (ORF) encoding GUS (*p1.7AVP1*::*GUS*) to monitor the spatiotemporal activity of the promoter in whole Col-0 Arabidopsis seedlings and adult plants. At the seedling stage, GUS activity is observed in shoot and root apical meristems, leaf primordia, cotyledons, and leaves (Fig. 1; Supplemental Fig. S1). GUS activity is also observed in source leaves and the source domain of leaves undergoing the sink-to-source transition. A strong GUS activity is evident in the vasculature of leaves, roots, and reproductive tissues (Fig. 1; Supplemental Fig. S1).

In adult soil-grown plants, there is preferential GUS activity in source leaves and the leaf and flower primordia (Fig. 2A; Supplemental Fig. S1A). The expression patterns showed GUS activity in mesophyll cells (Fig. 2, D and H) and a very conspicuous activity in the phloem tissue of leaf vascular bundles (Fig. 2). Immunogold localization studies showed evidence consistent with colocalization of the AVP1 and the bona fide PM marker plasma membrane intrinsic protein1 (PIP1) in Arabidopsis companion cell complexes (Paez-Valencia et al., 2011).

Physiological Parameters Consistent with Enhanced Photosynthate Production and Transport in *AVP1-1* Plants

AVP1-1 is a previously published Col-0 line overexpressing *AVP1* from the CaMV *35S* promoter. *AVP1-1* plants show increased shoot and root growth, drought tolerance, and nutrient use efficiency (Gaxiola et al., 2001; Yang et al., 2007). Both enhanced root growth in *AVP1-1* plants and the phloem-specific localization of AVP1 (Figs. 1 and 2) suggest a potential role in phloem loading. Col-0 and *AVP1-1* seedlings were photosynthetically labeled with $^{14}CO_2$, and ^{14}C was monitored by autoradiography. As shown in Figure 3A, roots of *AVP1-1* plants show about a 2-fold increase in ^{14}C labeling. In addition, the roots of *AVP1-1* seedlings released around 40% ($P \leq 0.01$) and 89% ($P \leq 0.05$) more protons than Col-0 during day and night hours, respectively, suggesting better sugar metabolism and ATP production in the *AVP1-1* roots (Fig. 3B). These data suggest that the up-regulation of *AVP1* is favoring the transport of reduced carbon from source to root.

Another phenotype associated with *AVP1* overexpression in Arabidopsis is an enhanced capacity for nutrient uptake (Yang et al., 2007; Undurraga et al., 2012). Regulation of the root K^+, NO_3^-, and inorganic phosphate transporter genes coordinates with photosynthesis and

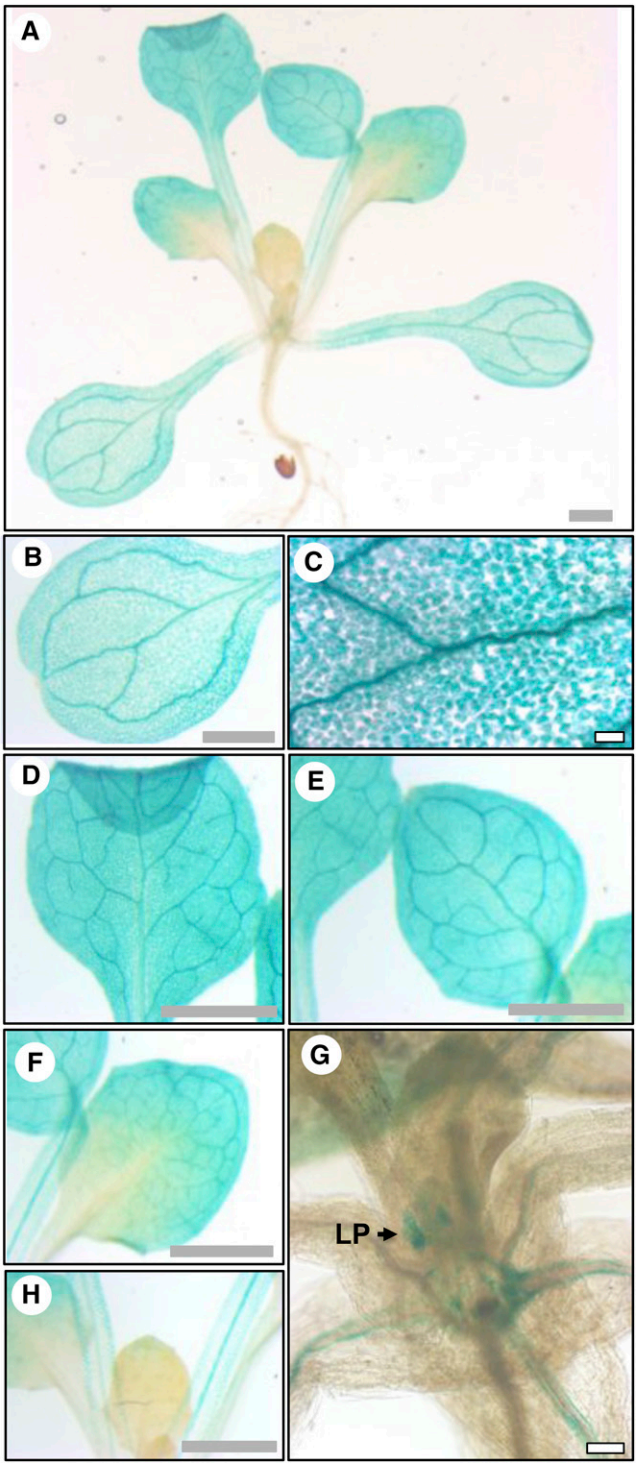

Figure 1. GUS staining patterns of an *AVP1* 1.7-kb promoter GUS reporter in Col-0 seedlings. Typical GUS staining of representative 15-d-old seedlings (A; $n = 3$ seedlings per trial; three independent trials) and details of cotyledon (B and C), source leaves (D and E), sink-to-source transition leaves (F), sink leaf (H), and leaf primordia (G). LP, Leaf primordia. Gray bars = 0.1 mm; white bars = 0.01 mm.

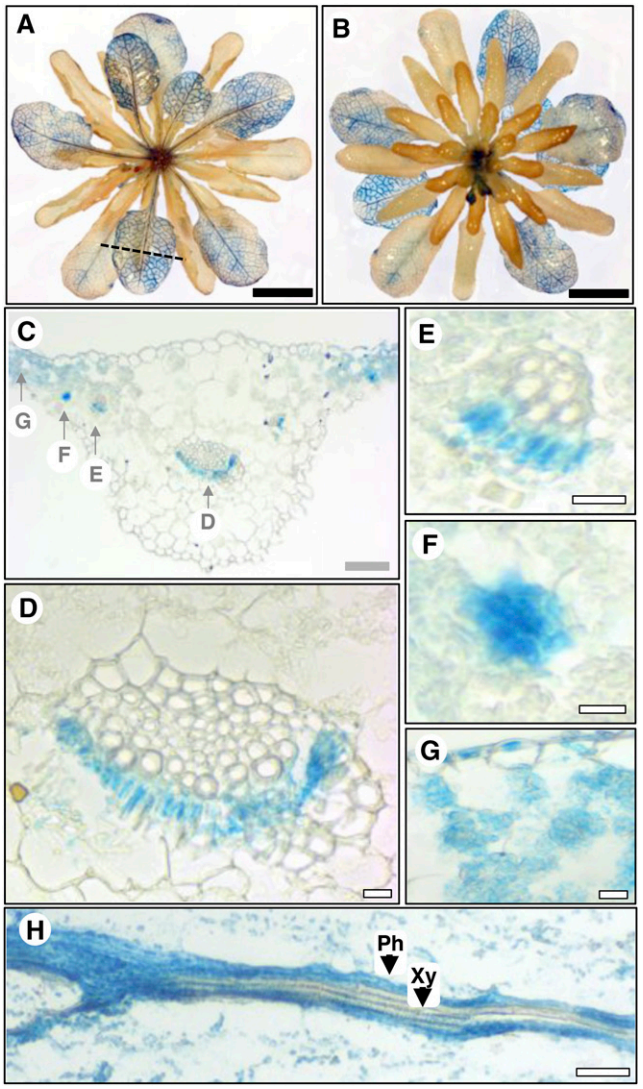

Figure 2. GUS staining patterns of an *AVP1* 1.7-kb promoter GUS reporter in Col-0 adult plants. Typical GUS staining of a 50-d-old plant grown under a 12-h/12-h day-night regimen. Bottom (A) and top (B) views. C, Transversal section (dotted line in A) of a representative source leaf from an adult plant ($n = 6$ leaves; from two independent plants). D to G, Details from C. H, Longitudinal section of a midvein. Ph, Phloem; Xy, xylem. Black bars = 1 cm; gray bars = 0.1 mm; white bars = 0.01 mm.

the carbon status of the plant (Lejay et al., 2008). We monitored *AVP1-1* and Col-0 plants for expression of four root ion transporters whose sugar induction has been extensively documented (Lejay et al., 2008). The expression levels of the four ion transporter genes tested, *POTASSIUM TRANSPORTER2* (*KUP2*; Arabidopsis *Potassium transporter2* [*AtKT2*] and *AT2G40540*), *NITRATE TRANSPORTER2.1* (*NRT2.1*; *Nitrate transporter2.1* [*ACH1*] and *AT1G08090*), *NRT2.4* (*AT5G60770*), and *PHOSPHATE TRANSPORTER1.4* (*PHT1.4*; Arabidopsis *Phosphate transporter2* [*AtKT2*] and *AT2G38940*), were at least 2-fold higher ($P \leq 0.01$) in *AVP1-1* than Col-0 roots (Fig. 3C). To further assess the potential role of AVP1 in phloem loading and transport, we evaluated seed production capacity. Seed yields from plants grown for 70 d under a 12-h/12-h day-night regimen showed that *AVP1-1* plants produced about 20% ($P \leq 0.05$) more seeds than Col-0 (Fig. 3D). These data are consistent with both the enhanced nutrient uptake capacity and a higher availability of reduced carbon in *AVP1-1* sinks.

The augmented biomass characteristic of these *AVP1-1* plants also suggests an enhanced carbon fixation capacity, and given that the amount of starch is directly correlated with the biomass of a plant (Sulpice et al., 2009), we documented the capacity of Col-0 and *AVP1-1* plants to accumulate starch during the day and mobilize it in the night. As expected, *AVP1-1* plants accumulated visibly more starch than Col-0 at the end of the day, and both mobilized most of it during the night period (Fig. 3E).

Both Ubiquitous and Phloem-Specific Up-Regulation of *AVP1* Enhance Shoot Biomass in Col-0

To further document the role of AVP1 in phloem of Arabidopsis, we generated transgenic plants carrying either a *p35S*::*AVP1* cassette for ubiquitous expression (Benfey and Chua, 1990) or a *Commelina Yellow Mottle Virus promoter* (*pCOYMV*)::*AVP1* cassette for phloem-specific expression (Fig. 4A). The *pCoYMV* promoter is from Commelina Yellow Mottle Virus and known to confer strong companion cell-specific expression (Medberry et al., 1992; Matsuda et al., 2002). It is also up-regulated by Suc, whereas another companion cell-specific promoter, Arabidopsis *SUCROSE-PROTON SYMPORTER2* (*pAtSUC2*), is repressed by Suc (Dasgupta et al., 2014). As expected, the *AVP1* mRNA expression levels in these transgenic lines are higher than in Col-0, and individual lines with each construct show differences in the *AVP1* transcript levels (Fig. 4, B and C). Plant biomass is enhanced in all transgenic lines, regardless of the promoter used (Fig. 4D).

The fact that both phloem-specific and ubiquitous *AVP1* expression enhanced Col-0 shoot biomass further emphasizes the potential role of this protein in phloem loading. In keeping with this idea, *AVP1-1* transgenic lines engineered with a phloem-specific *AVP1* silencing cassette (*pCoYMV*::$_{RNAi}$*AVP1*) were unable to grow in medium lacking Suc (Fig. 5, A and B; Supplemental Fig. S2). Whereas AVP1 immunohistochemical analysis of representative seedlings from *AVP1-1* showed strong expression in leaf primordia and vasculature, greatly reduced vascular staining was observed in three representative lines with phloem-specific *AVP1* silencing (Fig. 5C). These data suggest that *AVP1* expression in the phloem is necessary for healthy growth in medium without exogenous supplemental sugar.

A 244-bp Promoter of the *AVP1* Gene Is Sufficient to Direct Vascular Expression in Arabidopsis

Sequencing of the SALK 046492 line (hereafter called *avp1-2*) revealed a transfer DNA (T-DNA) insertion at the −244 site in the *AVP1* promoter relative to the ATG

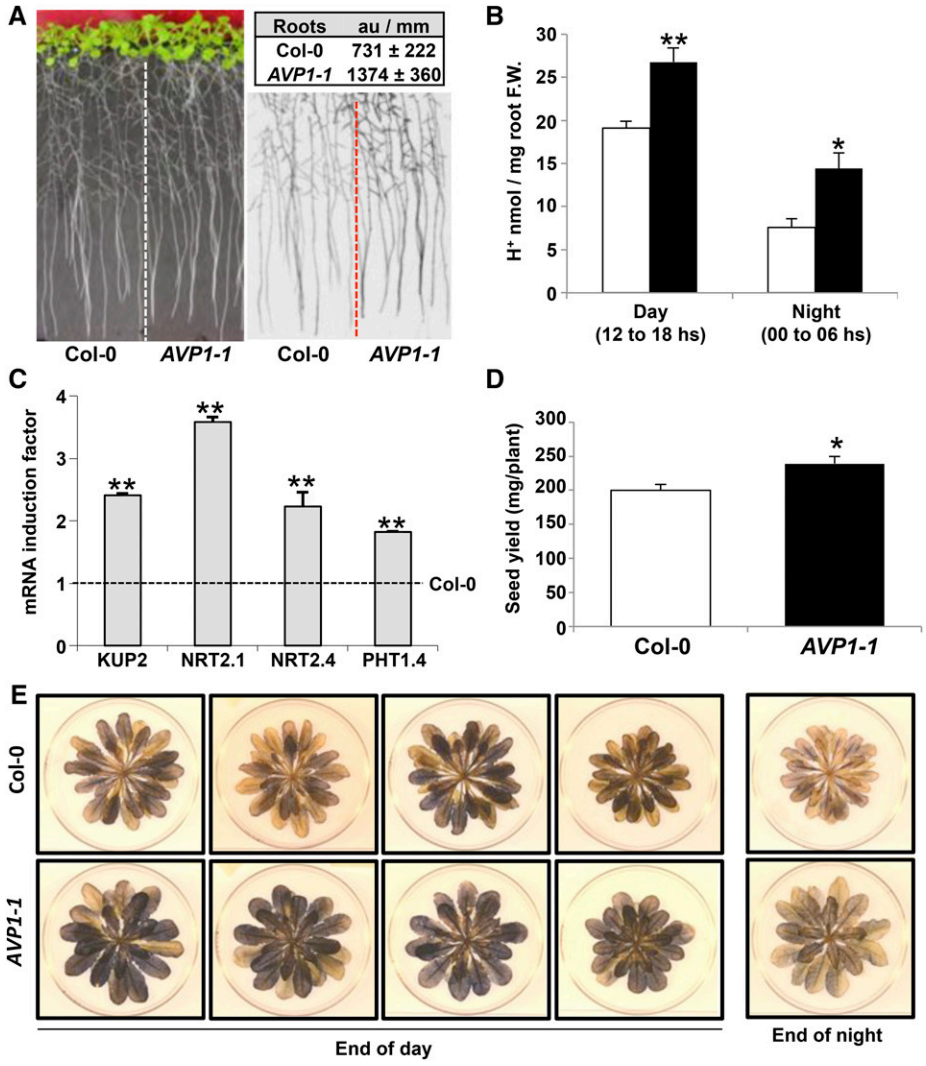

Figure 3. Indirect evidence of enhanced photoassimilate transport from source-to-sink tissues in *AVP1-1* plants. A, $^{14}CO_2$ labeling of plants grown in culture. Left, Plants before labeling. Right, Autoradiogram after 15 min of labeling and 60-m chase in normal air. Inset, ^{14}C in roots quantified as arbitrary units per millimeter ($n > 10$ roots measured; P value for t test $< 1 \times 10^{-5}$; one representative plate of four trials). B, Protons released from the roots during day and night hours by Col-0 (white bars) and *AVP1-1* (black bars) plants grown in liquid medium (means ± SE; $n = 6$ pools of 10 plants per line per time of day per trial; two independent trials). C, Expression of sugar-induced ion transporter genes (as indicated) in roots of *AVP1-1*. Data normalized to expression in Col-0 plants. Data are the average of three independent measurements ± SE; $n = 3$ plants per line per trial; five independent trials. D, Seed production in Col-0 and *AVP1-1* plants grown for 70 d in soil under a 12-h/12-h day-night cycle (means ± SE; $n = 7$ per line per trial; two independent trials). E, Lugol's staining of representative 50-d-old plants grown under a 12-h/12-h day-night regimen ($n = 8$ per line per trial; two independent trials). Significant differences relative to the wild type (Col-0) are based on Student's t test. F.W., Fresh weight; *, $P \leq 0.05$; **, $P \leq 0.01$.

start codon. Interestingly, we found six DNA-binding One Zinc Finger2 (DOF2) elements in this 244-bp promoter (Fig. 6A; Supplemental Fig. S3). DOF2 transcription factors recently emerged as part of the transcriptional regulatory network acting on the formation and functioning of the vascular tissues (Le Hir and Bellini, 2013). *AVP1* transcript levels in *avp1-2* plants were approximately 70% lower than in Col-0 (Fig. 6B). Congruently, the protein levels in *avp1-2* microsomes and tonoplast fractions are reduced compared with Col-0. Of note, AVP1 is barely detectable in the mutant tonoplast fraction (Fig. 6C). Immunohistochemistry on source leaves of adult *avp1-2* plants revealed a distinct AVP1 expression in the phloem of both mid and minor veins (Fig. 6D). Furthermore, PM localization of AVP1 in sieve element companion cell complexes was shown by immunogold labeling (Fig. 6E). This is significant, because despite the reduction in *AVP1* transcript (approximately 70%) and protein levels, phloem expression and healthy growth are retained, whereas phloem-specific silencing with *pCoYMV::*$_{RNAi}$*AVP1* resulted in severe stunting (Fig. 5). A comparison of growth and phenology between Col-0 and *avp1-2* plants showed that the shoot growth rate of these mutants is about 30% lower than that of Col-0 (Fig. 6, F and G). Accordingly, the shoot dry weight of 50-d-old soil-grown *avp1-2* plants is about 20% lower than that of Col-0 (Fig. 6H).

Phloem-Specific Expression of *E. coli ppa* Reveals a Key Role of PP_i in SE-CC Complexes

The facts that *avp1-2* mutants have reduced *AVP1* expression and that the protein is predominantly localized in the phloem further suggest a relevant role of this protein in this tissue (Fig. 6). Recent work has shown the PM localization of AVP1 in Col-0 SE-CC complexes (Paez-Valencia et al., 2011). Because of the large membrane potential across the PM of the SE-CC complex, the only thermodynamically feasible role that this enzyme can have at this interface is the reverse reaction as a PP_i synthase rather than its canonical forward reaction of a hydrolase (Davies, 1997). To help

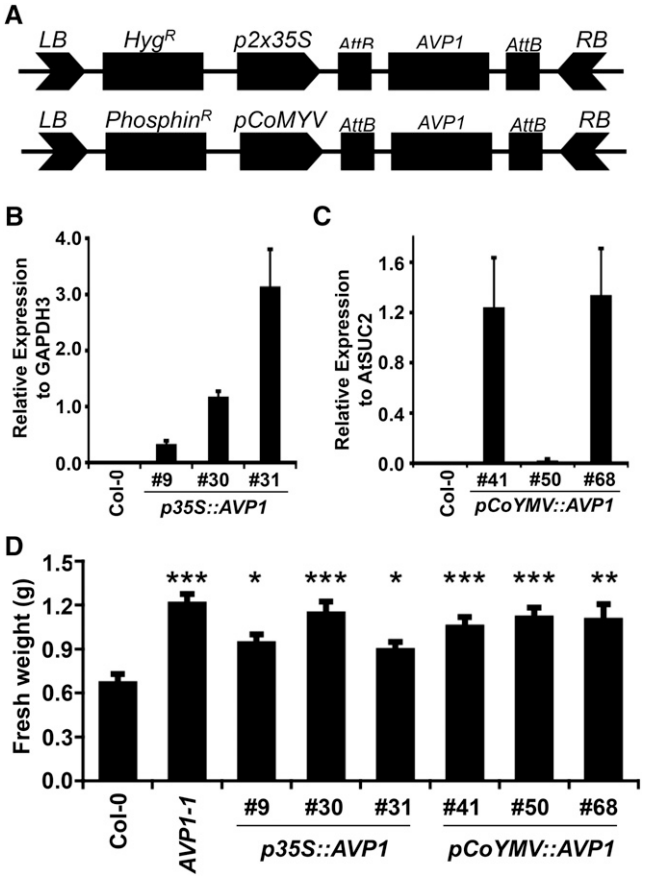

Figure 4. Impact of phloem-specific and constitutive overexpression of *AVP1* cDNA. A, Structure of T-DNA cassettes used to create transgenic plants expressing *AVP1* cDNA from the *CaMV 35S* promoter (with duplicated enhancer) in the *pMDC32* backbone and the *pCoYMV* promoter in a *pGPTV-bar* backbone (details in the text). LB, Left border; RB, right border. B and C, Fold accumulation of *AVP1* cDNA in rosettes of wild-type, *p35S*::*AVP1*, and *pCoYMV*::*AVP1* plants standardized to constitutive and phloem-specific housekeeping genes encoding *GAPDH3* and *SUC2*, respectively. For each line, $n = 3$ biological replicates; each was composed of four pooled plants, and qRT-PCR was conducted with technical duplicates. D, Fresh weight mass of rosettes from the indicated lines (means ± SE; $n = 6$ per line). Significant differences relative to the wild type (Col-0) are based on Student's t test. A second batch of plants grown several months earlier gave similar cDNA expression and fresh weight values; *, $P \leq 0.05$; **, $P \leq 0.01$; and ***, $P \leq 0.0001$.

resolve the role of AVP1 in the SE-CC complex as a PP_i synthase or a PPase, we tested the impact of overexpressing a nonreversible PPase activity. We expressed a well-characterized soluble PPase from *E. coli*, *ppa* (Lahti et al., 1988), in the phloem of *avp1-2* plants. T2 *avp1-2* plants engineered with the *pCoYMV*::*ppa* phloem-specific expression cassette (Supplemental Fig. S4) show a dramatic growth reduction (Fig. 7A; Supplemental Fig. S5, D and E). Earlier work showed that PP_i-dependent Suc hydrolysis is required for companion cell energization in tobacco plants (Lerchl et al., 1995). To monitor the expression of *E. coli ppa* in Arabidopsis, we raised ppa-specific antibodies (see "Materials and Methods"). As shown in Figure 7B, these antisera recognized a specific 25-kD band but did not cross react with any Col-0 proteins. Phloem expression of ppa from the pCoYMV promoter was confirmed by coimmunolocalization with the Arabidopsis H^+-ATPase (AHA3), which is recognized as having strong expression in phloem cells (Fig. 7C; DeWitt et al., 1991).

DISCUSSION

PM localization of AVP1 in SE-CC complexes has been extensively documented (Long et al., 1995; Ratajczak et al., 1999; Langhans et al., 2001; Paez-Valencia et al., 2011). Notably, overexpression of AVP1 and type I

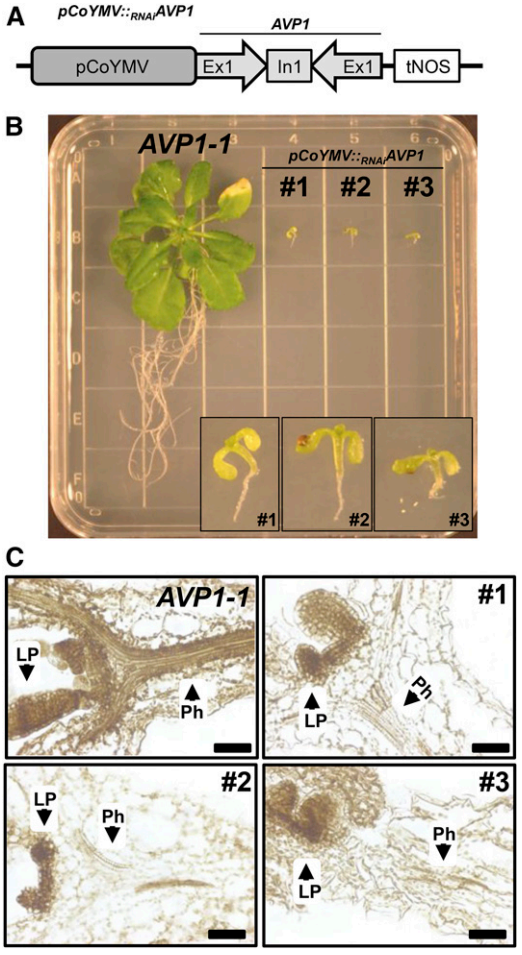

Figure 5. Phloem-specific *AVP1* silencing in *AVP1-1* plants. A, Expression cassette with the phloem-specific promoter *pCoYMV* driving the expression of $_{RNAi}$*AVP1*. B, *AVP1-1* and *pCoYMV*::$_{RNAi}$*AVP1* T2 lines (1–3) grown in the absence of Suc for 30 d under a 12-h/12-h day-night regimen. Zoomed images of T2 lines as indicated. C, Immunohistochemical analysis of AVP1 in representative *AVP1-1* (5 d old; $n = 10$ seedlings) and *pCoYMV*::$_{RNAi}$*AVP1* T2 lines 1 to 3 (15 d old; $n = 6$–10 seedlings from five independent *pCoYMV*::$_{RNAi}$*AVP1* lines). Note that all plants in C are at similar developmental stage (i.e. first true leaves emerging). LP, Leaf primordia; Ph, phloem. Black bars = 0.01 mm.

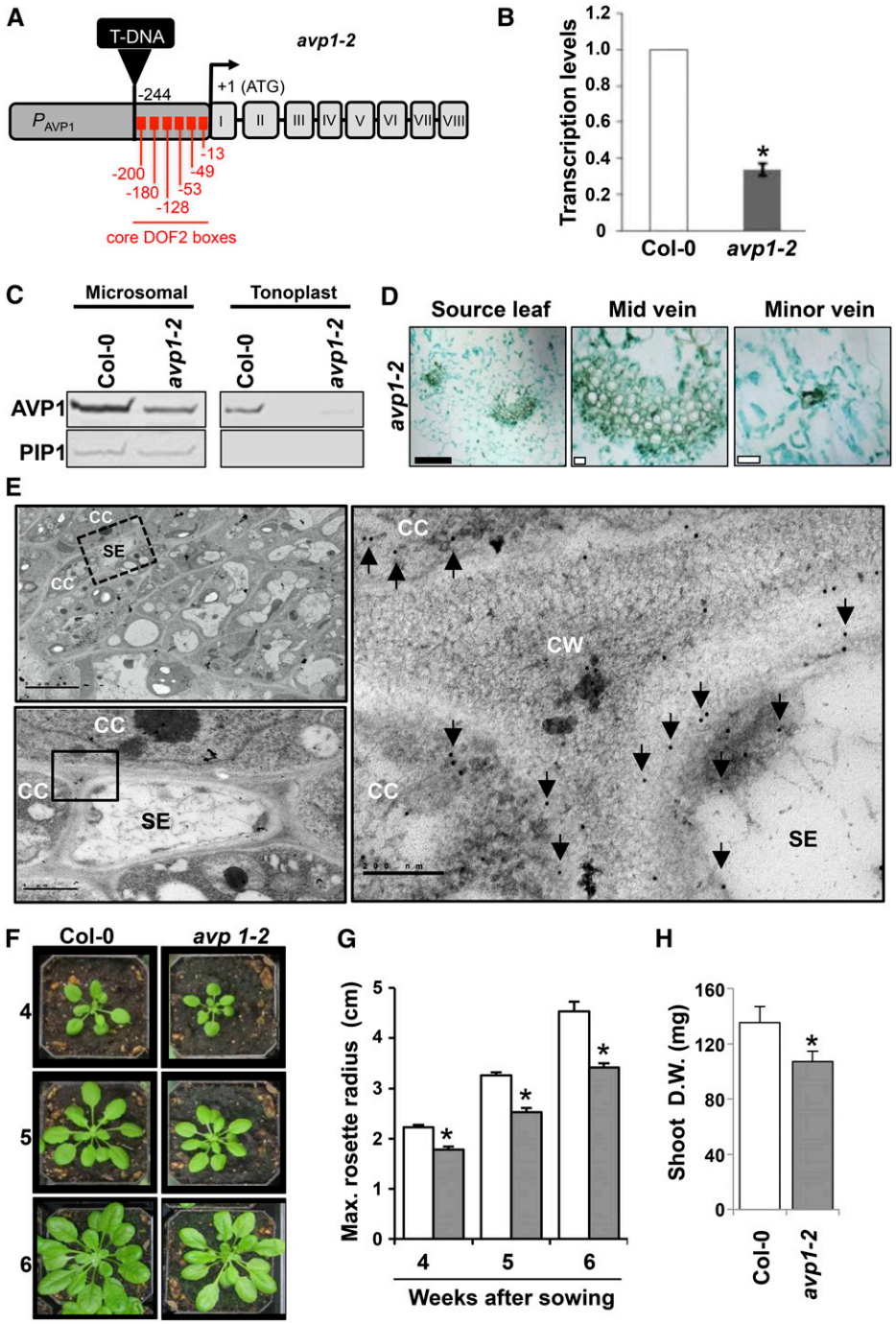

Figure 6. Molecular characterization and growth parameters of *avp1-2* (SALK 046492). A, Genomic structure of the *AVP1* gene showing the T-DNA insertion of the *avp1-2* line at −244 bp relative to the ATG start codon. Red squares indicate DOF2 elements. B, *AVP1* gene expression analysis in Col-0 and *avp1-2* plants was determined by qRT-PCR (means ± SE; $n = 4$ plants per line; the relative mRNA levels were normalized to the *UBQ10* gene). C, Immunoblots of AVP1 and PIP1 from total microsomal and tonoplast fractions extracted from Col-0 and *avp1-2* plants. D, Immunohistochemical analysis of AVP1 expression in transversal sections of *avp1-2* adult source leaves. Black bars = 0.1 mm; white bars = 0.01 mm. E, Ultrastructural details of *avp1-2* minor vein. Upper left, Transverse sections treated with anti-AHA3 sera and gold-conjugated secondary antibody. Lower left and right, Higher magnification of dotted and solid boxed regions, respectively. Arrows show gold particles localized at the PM of companion cells and sieve elements. F and G, Phenology and growth of Col-0 (white bars) and *avp1-2* (gray bars) plants at different times after sowing as indicated. Maximum rosette radius: means ± SE; $n = 20$ plants per line (pot width = 5.8 cm). H, Shoot dry weight of 50-d-old plants (means ± SE; $n = 6$ plants per line; two independent trials). Significant differences relative to Col-0 are based on Student's *t* test. CC, Companion cell; CW, cell wall; D.W., dry weight; SE, sieve element; *, $P \leq 0.05$.

H^+-PPases in several different crops is shown to increase shoot and root biomass (Li et al., 2005; Yang et al., 2007; Bao et al., 2008; Lv et al., 2008; Pasapula et al., 2011; Arif et al., 2013; Paez-Valencia et al., 2013; Schilling et al., 2014). Some of these transgenic plants also have enhanced rhizosphere acidification capacity and nutrient use efficiencies (Yang et al., 2007; Pei et al., 2012; Undurraga et al., 2012; Paez-Valencia et al., 2013; Li et al., 2014). These phenotypes suggest that H^+-PPase up-regulation elicits an increased production and mobilization of photoassimilates. In this work, we present a body of evidence that supports a fundamental role of AVP1 in phloem loading and transport of photoassimilates in Arabidopsis.

To learn about the spatiotemporal expression pattern of the *H^+-PPase* gene in Arabidopsis, we analyzed the activity of a 1.7-kb *AVP1* promoter fused to the *uidA* gene encoding GUS. GUS activity was monitored in seedlings (Fig. 1; Supplemental Fig. S1) and adult plants (Fig. 2; Supplemental Fig. S1). A conspicuous vascular expression was evident in both developmental stages, and transversal leaf sections revealed that it is phloem

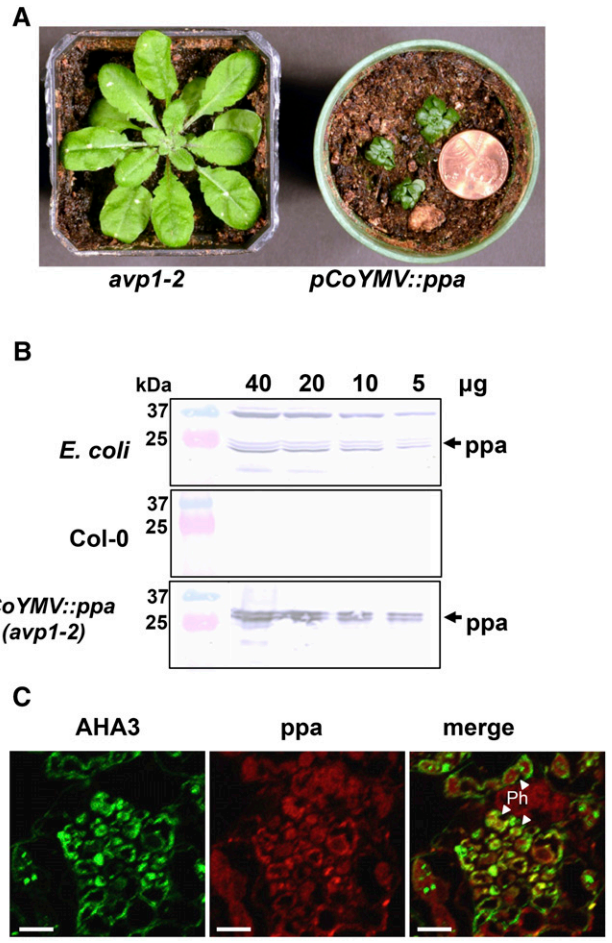

Figure 7. Effect of the phloem-specific expression of an *E. coli* soluble ppa in the *avp1-2* mutant. A, Rosettes of representative *avp1-2* and T2 *avp1-2 pCoYMV::ppa* plants (40 and 60 d old, respectively. Note that five independent T2 *avp1-2 pCoYMV::ppa* transgenic lines were analyzed, and the phenotypes were similar. Pot width = 5.8 cm. B, Immunoblots of *E. coli*-soluble ppa (different amounts of the protein extracts as indicated) from *E. coli* and Col-0 and T2 *avp1-2 pCoYMV::ppa* plants. C, Coimmunolabeling of AHA3 (green) and ppa (red) in minor veins of T2 *avp1-2 pCoYMV::ppa* leaves. Ph, Phloem. Bars = 0.01 mm.

specific. Of note, leaves of 15-d-old seedlings (Fig. 1) show a distinct sink-to-source transition pattern that mimics that of the PM-localized Suc-H^+ symporter, SUC2 (Truernit and Sauer, 1995; Imlau et al., 1999; Schneidereit et al., 2008). The sink-to-source transition starts at the tip of expanding young leaves and proceeds toward the base (Turgeon and Webb, 1973; Wright et al., 2003). SUC2 and orthologs are essential transporters required for phloem loading of Suc in apoplasmic loaders like Arabidopsis, and they are commonly used markers of the sink-to-source transition in leaves (Wright et al., 2003; Schneidereit et al., 2008). The closely correlated expression patterns of *SUC2* and *AVP1* further suggest that AVP1 is involved in the phloem-loading process. It is worth mentioning that an earlier report using a 1.4-kb *AVP1* promoter fused to GUS showed vascular and mesophyll expression (Mitsuda et al., 2001). Interestingly, this group contends that, although mesophyll expression is repressed by light, vascular expression is not (Mitsuda et al., 2001). In addition, we see strong GUS activity in sink tissues (root and shoot meristems, hypocotyls, stamen, pistil, and leaf primordia; Figs. 1 and 2; Supplemental Fig. S1). These results are consistent with the role of H^+-PPases in hydrolyzing PP_i generated as by-products of biopolymer synthesis (nucleic acids, cellulose, etc.) in rapidly growing cells, which if allowed to accumulate, would inhibit these biosynthetic reactions (Gaxiola et al., 2007).

Different physiological parameters involved with photoassimilate production and transport were evaluated in *AVP1-1* plants (Gaxiola et al., 2001; Li et al., 2005; Yang et al., 2007). A pulse with $^{14}CO_2$ shows that AVP1 up-regulation enhances the amount of reduced carbon allocated to the roots of transgenic seedlings (Fig. 3A). Augmented root proton extrusion capacity was also evident during both the day and the night (Fig. 3B). Furthermore, expression of well-characterized Suc-induced root ion transporters (*KUP2*, *NRT2.1*, *NRT2.4*, and *PHT1.4*) was enhanced in these plants (Fig. 3C). *AVP1-1* plants also have significantly higher seed yield (Fig. 3D). In an apoplasmic loader like Arabidopsis, increased supply of sugars to sinks tissues is directly correlated with Suc phloem loading (Ruan, 2014). Increments in reduced carbon production (i.e. photosynthesis) are not enough to increase availability in sinks; enhanced phloem loading and transport are also required. We reason that *AVP1* up-regulation improves apoplasmic loading by providing more PP_i substrate for Suc oxidation, resulting in more ATP for the maintenance of the PMF across the PM through the PM ATPase.

Interestingly, rhizosphere acidification capacity is reduced during the night in both *AVP1-1* and Col-0 (Fig. 3B). This could be explained by the fact that root growth occurs mostly at night (Yazdanbakhsh et al., 2011; Kircher and Schopfer, 2012; Müller et al., 2014), and the photoassimilates are redirected, in part, to build root biomass. It is worth emphasizing that the nocturnal acidification capacity displayed by the *AVP1-1* plants is still significantly higher than in Col-0. Starch content has been identified as the major integrator of plant biomass (Sulpice et al., 2009). In agreement, *AVP1-1* plants have stronger starch staining than Col-0 at the end of the day (Fig. 3E). Thus, *AVP1-1* plants are not only mobilizing more photoassimilates but also, storing more starch in leaves. Moreover, most of this starch is mobilized at night to presumably feed the root carbon requirements, enhancing nocturnal root acidification and growth.

To further analyze the role of H^+-PPase in the SE-CC complexes, we generated transgenic plants with phloem-specific *AVP1* up- (Fig. 4A; Col-0 background) and down-regulation (Fig. 5A; *AVP1-1* background). We used the well-characterized promoter element from Commelina Yellow Mottle Virus (*pCoYMV*) that directs expression specifically in the companion cells (Medberry and Olszewski, 1993; Dasgupta et al., 2014). All three independent *pCoYMV::AVP1* lines showed a

significant increase in shoot biomass relative to Col-0, comparable with the biomass developed by four independent *p35S*::*AVP1* lines, including *AVP1-1* (Fig. 4D). These results show that phloem-specific *AVP1* overexpression is sufficient to enhance biomass in Arabidopsis, even under minimal increase in transcript levels (Fig. 4). A detailed characterization of *p35S*::*AVP1* and *pCoYMV*::*AVP1* lines is seen in the work by A.S. Khadilkar, U.P. Yadav, C. Salazar, V. Shulaev, J. Paez-Valencia, R.A. Gaxiola, and B.G. Ayre, (unpublished data).

Phloem-specific *AVP1* RNAi (*pCoYMV*::$_{RNAi}$*AVP1*) lines generated in *AVP1-1* background further emphasize the requirement of the H^+-PPase in phloem function (Fig. 5; Supplemental Fig. S2). In stark contrast with the *AVP1-1* phenotypes, the transgenic lines with phloem-specific silencing showed profound growth impairment in the absence of Suc supplementation in the growth medium (Fig. 5B; Supplemental Fig. S2), whereas medium with Suc partially restored growth to *pCoYMV*::$_{RNAi}$*AVP1* plants (data not shown). This is consistent with impaired phloem loading and Suc transport in *pCoYMV*::$_{RNAi}$*AVP1* lines. In addition, similarities in the spatial and temporal expression patterns conferred by the *AVP1* promoter (Fig. 1A) and the promoter of SUC2 encoding the primary if not the exclusive Suc-H^+ symporter involved in Arabidopsis phloem loading of Suc (Truernit and Sauer, 1995; Gottwald et al., 2000; Srivastava et al., 2008) further suggest a prominent role for AVP1 in phloem loading and transport. The stunted growth in *pCoYMV*::$_{RNAi}$*AVP1* lines resembles *suc2* knockout plants (Gottwald et al., 2000).

An *AVP1* mutant, *Vacuolar proton pyrophosphatase1-1* (*vhp1-1*; Ferjani et al., 2011; Segami et al., 2014), also showed a significant growth reduction in Suc-depleted medium but no growth impairment under Suc supplementation (Supplemental Fig. S5). Of note, this *vhp1-1* mutant retains approximately 25% of PPase activity in total membrane fractions compared with Col-0 (Segami et al., 2014). Other *AVP1* mutants (*fugu5-1*, *fugu5-2*, and *fugu5-3*) without detectable tonoplast PPase activity have been reported (Ferjani et al., 2011). It is worth mentioning that the main phenotype reported for these mutants is a mild reduction in cotyledon size in early heterotrophic stages (Ferjani et al., 2011). However, beyond this stage, a notable reduction in shoot development was evident when grown in soil (Supplemental Fig. S3). These phenotypes are consistent with problems in photosynthate partitioning. Additional characterization of the above *fugu* mutants in autotrophic developmental stages, where phloem loading becomes critical, is needed.

Unlike *pCoYMV*::$_{RNAi}$*AVP1* and *vhp1-1* mutants, both *35S* ethanol-inducible $_{RNAi}$*AVP1* and *avp1-1* lines that show shoot abnormalities and strong inhibition of root growth could not be rescued with Suc supplementation (Li et al., 2005). These data suggest that AVP1 also has essential functions independent of phloem Suc loading. These are probably related to AVP1 in the vacuolar and prevacuolar compartments mediating PP_i hydrolysis and lumen acidification. The discrepancy in these Suc-dependent phenotypes warrants further experiments.

Interestingly, compared with Col-0, the *avp1-2* line showed only a mild growth reduction, despite having a short promoter (244 bp) and only about 30% *AVP1* expression (Fig. 6). This 244-bp promoter fragment has six DOF2 elements (Supplemental Fig. S4). DOF2 elements (AAAG or CTTT) are the core binding sites for DOF transcription factors (Noguero et al., 2013) that are positive regulators required in the formation and functioning of vascular tissues, including those of Arabidopsis (Ward et al., 1998; Zhao et al., 2005; Le Hir and Bellini, 2013). DOF2 elements are also present in the essential 241-bp *SUC2* promoter fragment that drives phloem-specific SUC2 expression in Arabidopsis (Schneidereit et al., 2008), and the 244-bp promoter is sufficient to drive *AVP1* expression in the phloem (Fig. 6, C–E). A severe impairment of the hydrolytic and proton-translocating activities of the H^+-PPase in this *avp1-2* mutant has been previously reported (http://abstracts.aspb.org/pb2004/public/M24/9123.html). These findings are in agreement with the reduced levels of AVP1 protein detected in the tonoplast fractions of *avp1-2* plants (Fig. 6C). Importantly, AVP1 immunogold labeling in these plants showed normal PM localization in SE-CC complexes, which has been reported previously in Arabidopsis (Fig. 6E; Paez-Valencia et al., 2011).

The phloem-specific expression of the soluble PPase from *E. coli*, ppa (Lahti et al., 1988), in *avp1-2* plants resulted in a dwarf phenotype (Fig. 7A; Supplemental Fig. S4). This result agrees with a previous work that showed a similar effect in transgenic tobacco plants expressing the same ppa enzyme in the SE-CC complexes (Lerchl et al., 1995). Clearly, the lack of PP_i in the phloem system is detrimental for normal growth in apoplasmic loaders. Therefore, these results are consistent with the thermodynamically sound role of AVP1 as a PP_i synthase in the PM of SE-CC complexes (Gaxiola et al., 2012).

A better understanding of carbon partitioning is essential for crop improvement. In this work, we present evidence consistent with a PP_i synthase function for the PM-localized AVP1 in SE-CC complexes in Arabidopsis. Our results agree with the involvement of this enzyme in the maintenance of PP_i homeostasis in companion cells with direct implications in phloem function.

MATERIALS AND METHODS

Plant Material and Growth Conditions

The plant materials used in this work are as follows: Col-0, gain-of-function *AVP1-1* line (Gaxiola et al., 2001), T-DNA promoter insertion line *avp1-2* (SALK 046492), transgenic reporter line *p1.7AVP1*::*GUS* (Yang et al., 2007), *pCoYMV*::*AVP1* and *p35S*::*AVP1* (Col-0 background; this work), *pCoYMV*::$_{RNAi}$*AVP1* (in an *AVP1-1* background), *pCoYMV*::*ppa* (in an *avp1-2* background), *fugu5-1* (Ferjani et al., 2011), and *vhp1-1* (Segami et al., 2014).

When planted in soil, plants were grown in Sun Gro Sunshine LP5 Mix Plug in growth chambers at 21°C with a 12-h-light/12-h-dark cycle. When aseptic growth was required, plants were grown in one-half-strength Murashige and

Skoog (MS) salt mixtures (GIBCO/BRL) at 25°C under a 12-h-light/12-h-dark cycle. The medium was supplemented with 2% (w/v) Suc (when indicated) and 1% (w/v) agar. In all cases, before sowing, seeds were stratified at 4°C for 2 d. For experiments requiring sterility, seeds were surface sterilized by soaking them in 30% (v/v) commercial bleach and 0.05% (v/v) Tween 20 for 15 min and rinsed four times with sterile water.

Constructs, Transformation, and Selection

AVP1 complementary DNA (cDNA) was amplified by PCR from *pRT103-AVP1* (Gaxiola et al., 2001) using forward oligonucleotide AVP1-F (5′-CACCATGGTGGCGCCTGCTTTGTTAC-3′) and reverse oligonucleotide AVP1-R (5′-GAAGTACTTGAAAAGGATACCACC-3′). Phusion Hot Start Polymerase (NEB) was used according to the manufacturer's instructions. The PCR product was cloned with a pENTR/D-TOPO Cloning Kit (Invitrogen), resulting in *pENTR-AVP1*. *pENTR-AVP1* was recombined with pMDC32 (Curtis and Grossniklaus, 2003) using the Gateway LR Clonase II Enzyme Mix (Invitrogen) to generate pMDC32::AVP1. pMDC32 contains a duplicated 35S enhancer element (Curtis and Grossniklaus, 2003). *pENTR::AVP1* was recombined with *pGPTV::CoYMVp::cmr::ccdB* (Dasgupta et al., 2014) to get *pGPTV::CoYMVp::AVP1*. These vectors were electroporated into *Agrobacterium tumefaciens* strain GV3101mp90.

Wild-type Col-0 (Arabidopsis Biological Resource Center stock no. CS-70000) was transformed with the above constructs by the floral dip method (Clough and Bent, 1998). T1 generation seeds of plants transformed with *pMDC32::AVP1* were selected on sterile one-half-strength MS medium (Phytotechnology Laboratories) containing 40 mg L^{-1} hygromycin. Seeds were germinated in the dark and grown for 5 d; resistant seedlings were selected based on their longer hypocotyls (Harrison et al., 2006) and transferred to Fafard 3B potting mix (Sun Gro Horticulture). For selecting plants transformed with *pGPTV:pCoYMV:AVP1*, T1 seeds were germinated on Fafard 3B potting soil and sprayed with 20 mg L^{-1} glufosinate ammonia (Finale; Farnam Companies) postgermination. Twenty-five or more independent lines were identified for both *pCoYMV::AVP1* and *p35S::AVP1* cassettes. Lack of segregation of the resistance marker in the T3 generation was used to identify homozygous lines. From these, three representative lines for each construct were selected for further experiments based on cDNA expression and growth morphology.

The *pCoYMV::$_{RNAi}$AVP1* construct was generated using the *AVP1* silencing cassette reported previously (Li et al., 2005) cloned behind *pCoYMV* (Dasgupta et al., 2014). This expression cassette was cloned into pClean-G146, and the resulting vector was cotransformed with pClean-S166 (Thole et al., 2007) into *A. tumefaciens* GV3101mp90. Selection of positive transformants was done as described previously (Thole et al., 2007).

To generate the *pCoYMV::ppa* construct, total chromosomal DNA from *Escherichia coli K-12* was isolated. The *ppa* ORF was amplified (Supplemental Table S1 shows primers). Amplicons were digested with *Nco*I and *Sma*I and directionally cloned into pRT103 (Töpfer et al., 1987). Subsequently, the *ppa* ORF was digested with *Nco*I and *Xba*I and cloned between the CoYMV promoter and octopine synthase polyadenylation signal in the pClean-G146 binary plasmid (Thole et al., 2007). This plasmid was cotransformed with pClean-S166 (Thole et al., 2007) into *A. tumefaciens* GV3101mp90. Selection of positive transformants was done as described previously (Thole et al., 2007).

A. tumefaciens carrying the above plasmids was used to transform Arabidopsis (*Arabidopsis thaliana*) Col-0, *AVP1-1*, or *avp1-2* (SALK 046492) by the floral dip method (Desfeux et al., 2000).

Histochemical GUS Staining

Seedlings and adult plants from two T3 independent lines (Yang et al., 2007) were infiltrated with staining solution (50 mM sodium phosphate buffer, pH 7.0, 0.5 mM potassium ferrocyanide, 0.5 mM potassium ferricyanide, and 2 mg mL^{-1} 5-bromo-4-chloro-3-indolyl-β-D-GlcA; SIGMA-Aldrich) in a vacuum chamber for 2 h and subsequently incubated at 37°C for 24 h. Then, all tissues were fixed in 3.7% (v/v) formaldehyde, 50% (v/v) ethanol, and 5% (v/v) acetic acid for 3 h at room temperature and cleared in 70% (v/v) ethanol for several days. After that, the tissues were rehydrated in water and mounted on glass slides with glycerol. For sectioning, fixed material was dehydrated in a graded ethanol series (50%, 60%, 70%, 80%, 90%, and 100% [v/v]), and absolute ethanol was replaced by *tert*-butanol (SIGMA-Aldrich). Tissues were embedded in paraplast at 60°C. The embedded tissue was sliced with a microtome into 30-μm sections and placed onto poly-Lys-coated slides (Denville Scientific). Sections on slides were deparaffinized in *tert*-butanol, hydrated in a graded alcohol series (100%, 90%, 80%, 70%, 60%, 50%, and 30% [v/v] distilled, deionized water), and mounted with glycerol. Samples were analyzed under an Olympus BX40 Microscope or an Olympus SZx7 Stereomicroscope and photographed with an Infinity2 Camera (Lumenara Corp.).

$^{14}CO_2$ Labeling

In brief, seeds were arranged on sterile filter paper dyed black with India ink (for visualizing roots; we see no toxicity) and placed on top of MS nutrient medium with 1% (w/v) Suc. The plates were incubated 60° from horizontal so that the roots grew down the black paper. After 1 week, the paper with seedlings was transferred to Suc-free medium for 2 weeks, with a second transfer to fresh medium after the first 1 week. The paper with plants was transferred to a clean plate, the lid was sealed in place with vacuum grease, and this chamber was placed below a 400-W metal halide lamp. The leaves were photosynthetically labeled with $^{14}CO_2$ created by acidifying 5 μCi of [^{14}C]Na-bicarbonate. After the desired labeling and chase period (15 and 60 min, respectively), the plants and supporting filter paper were placed between two sheets of protective paper, flash frozen, and lyophilized at −35°C to prevent diffusion of transported label. The plants were exposed to Kodak BioMAX MR Film; the autoradiograph was scanned on a flatbed scanner, and density was established with ImageJ. Four plates were labeled in this manner, with one representative plate presented in Figure 3.

Acidification Assay

Seeds were germinated and grown aseptically on vertical agar plates for 5 d. Then, seedlings (10 per point) were transplanted to flasks with 4 mL of liquid medium (one-half-strength MS and 1% [w/v] Suc) and grown for 2 weeks. Before the acidification assay, roots were washed with the assay solution (one-quarter-strength MS and 2 mM MES buffer, pH 6.8) for 5 min. Acidification assay was performed in fresh assay solution during either the day (from 12–6 PM) or the night (from 12–6 AM). H^+ released to the medium was calculated by the difference between the initial and final pH and standardized to the total root fresh weight.

Quantitative Real-Time PCR

AVP1

Total RNA was extracted from rosette leaves of adult Col-0 and *avp1-2* plants using Trizol reagent following the manufacturer's instructions. To rule out genomic contamination, a PCR with primers designed on intron sequences of Actin7 (ACT7; At5g09810; ACT7-FOR, 5′-GAC ATG GAA AAG ATA TGG CAT AC AC-3′; ACT7-REV, 5′-AGA TCC TTC CTG TGG CAT CAC AC-3′) was carried out. After measuring RNA concentrations, samples were adjusted to the same value for subsequent cDNA synthesis reactions. Reverse transcription was carried out using the RETROscript Kit (Ambion). Quantitative real-time (qRT)-PCR analysis was done in optical 96-well plates with a MyiQ Single-Color Real-Time PCR Detection System (Bio-Rad) using SYBR Green to monitor double-strand DNA synthesis. The primers used are listed in Supplemental Table S1. Each reaction contained 1 μL of cDNA, 0.5 μL of each of two gene-specific primers, and 10 μL of 2× iQ SYBR Green Super Mix Reagent (Bio-Rad) in a final volume of 20 μL. Threshold cycle (Ct) values were calculated using Optical System Software, version 1.0 for MyiQ (Bio-Rad). Subsequently, Ct values were normalized for differences in double-strand DNA synthesis using the *Ubiquitin10* (*UBQ10*) Ct values. The relative value for expression levels of each gene was calculated by the equation $Y = 2^{-\Delta\Delta Ct}$, where ΔCt is the difference between control and target products [$\Delta Ct = Ct_{(AVP1)} - Ct_{(UBQ10)}$] and $\Delta\Delta Ct = \Delta Ct_{(transgenic)} - \Delta Ct_{(the\ wild\ type)}$. Thus, the calculated relative expression values are normalized to wild-type expression levels (the wild type = 1). Three different technical replicates and two independent sets of plants were used for analysis.

Sugar-Induced Ion Transporter Genes (*KUP2*, *NRT2.1*, *NRT2.4*, and *PHT1.4*)

Total RNA was extracted from roots of adult Col-0 and *AVP1-1* plants grown under hydroponic conditions as described previously (Lejay et al., 2008). The qRT-PCR analysis of ion transporter genes was performed as above, with the exception of the housekeeping gene, *Clathrin1* (At4g24550; Supplemental Table S1).

AVP1 in Transgenic Lines (*p35S::AVP1* and *CoYMVp::AVP1*)

For qRT-PCR on p35S::AVP1 lines 9, 30, and 31 and CoYMVp::AVP1 lines 41, 50, and 68, four well-spaced plants were grown in 3.5-in square pots under the conditions described above but using Fafard 3B Mix as the potting medium. Three pools (each containing four rosettes of 28-d-old plants from different pots) were ground at liquid nitrogen temperatures, and total RNA was isolated from 50 mg of each pool using Trizol and treated with DNase; 1 μg of total RNA was reverse transcribed with either Superscript III (Life Technologies) or GoScript (Promega). qRT-PCR was carried out in duplicate for each of the three pools using GO Taq qPCR Mix (Promega) on an Applied Biosystems ViiA 7 (Life Technologies) with 2 min of denaturation at 95°C followed by 40 cycles of 95°C for 10 s, 65°C for 30 s, and 70°C for 30 s. Final melting curves were obtained to confirm a single PCR product. Expression of the *AVP1* cDNA transgene was normalized against *Glyceraldehyde-3-phosphate dehydrogenase* (*GAPDH3*) for the *p35S::AVP1* lines and against *AtSUC2* for the phloem-specific *pCoYMV::AVP1* overexpression lines with *AtSUC2*. Three biological and two technical replicates were used for analysis. The gene-specific primers used are listed in Supplemental Table S1.

AVP1 Immunolocalization

Arabidopsis seedlings or source leaves (as indicated) were fixed in 3.7% (v/v) formaldehyde, 50% (v/v) ethanol, and 5% (v/v) acetic acid for either 3 h at room temperature (seedlings) or overnight at 4°C (leaves). Fixed material was dehydrated in a graded ethanol series (50%, 60%, 70%, 80%, 90%, and 100% [v/v]), and absolute ethanol was replaced by a histological clearing agent (xylene; SIGMA-Aldrich). Tissues were embedded in paraplast at 60°C. The embedded tissue was sliced into 10- to 15-μm sections and placed onto poly-Lys-coated slides. Sections were deparaffinized in xylene, hydrated in graded alcohol (100%, 90%, 80%, 70%, 60%, 50% [v/v], and 30% [v/v] distilled, deionized water), and pretreated with Antigen Retrieval Solution (BioGenex) under a steamer at 65°C for 20 min. Endogenous peroxidase activity was quenched with 3% (v/v) hydrogen peroxide, and the slides were treated with Power Universal Reagent (BioGenex) to reduce nonspecific binding and incubated with polyclonal anti-H^+-PPase antibody (Park et al., 2005). Controls were done with preimmune sera at a 1:1,000 dilution in phosphate-buffered saline (PBS) for all samples. Then, three rinses with 0.1% (v/v) PBS Tween were followed by incubation with the DAKO EnVision System (DAKO) following the manufacturer's instructions.

Microsomal Fraction and Tonoplast Isolation

Plant leaf tissue was homogenized in a buffer containing 250 mM sorbitol, 50 mM HEPES-1,3-bis(tris[hydroxymethyl]methylamino) propane, pH 7.4 (SIGMA-Aldrich), 25 mM ascrobic acid, 1 mM dithiothreitol (DTT; Fluka), 6 mM EGTA (SIGMA-Aldrich), 1.2% (w/v) Polyvinylpyrrolidone-40 (SIGMA-Aldrich), and protease inhibitor cocktail (Complete EDTA-Free; Roche). A 1:2 (w/v) ratio of tissue and homogenization medium was used. The homogenization medium was filtered through four layers of cheesecloth and centrifuged at 10,000*g* for 15 min (JA 30.50 Ti Rotor; Beckman). The supernatant was recovered and centrifuged at 60,000*g* for 30 min (SW 28 Rotor; Beckman), and microsomal fractions were suspended in 250 mM sorbitol, 25 mM HEPES-Bis-Tris propane, pH 7.4, 1 mM DTT, and protease inhibitor cocktail (Complete EDTA-Free; Roche). Separation of tonoplast fractions was done with a three-step dextran gradient as previously described (Schumaker and Sze, 1985). Protein concentration was measured with BCA Reagent (Thermo) according to the manufacturer's instructions.

Total Protein Isolation of *E. coli*, Col-0, and P_{CoYMV}::*sPPase* Lines

Homogenates of *E. coli* and plant shoots of Col-0 and P_{CoYMV}::*sPPase* (*avp1-2* background) were prepared in a homogenization buffer: 50 mM HEPES, pH 7.4, 250 mM D-sorbitol, 6 mM EGTA, 1 mM DTT, 0.2% (w/w) bovine serum albumin, and protease inhibitor cocktail (Complete EDTA-Free; Roche).

Antibody Production

The synthetic peptide N-terminal (NH2)-CIKDVNDLPELLKAQIAH corresponding to *E. coli*-soluble ppa (EC 3.1.3.1) was conjugated to keyhole limpet hemocyanin. Antibody production in rabbit was as described previously (Paez-Valencia et al., 2011). The synthetic peptide (NH2)-CTISKDRVKPSPTPDS corresponding to positions 690 to 704 of AHA3 (At5g57350; Kobae et al., 2004) was conjugated to keyhole limpet hemocyanin. Antibody production in mouse was as described previously (Paez-Valencia et al., 2011).

Western Blot

Protein samples were separated by 10% (w/v) SDS-PAGE. After electrophoresis, gels were either stained with Coomassie Brilliant Blue R-250 (SIGMA-Aldrich) or transferred to Immobilon-P membranes (Millipore). After blocking with 0.1% (v/v) Tris-buffered saline-Tween 20 and 5% (w/v) defatted milk, membranes were incubated overnight at 4°C with polyclonal sera raised in rabbits against the following antigens: soluble PPase (this work), H^+-PPase (Park et al., 2005), and PIP1 (Paez-Valencia et al., 2011). After 1 h of incubation with the secondary goat anti-rabbit IgG coupled to alkaline phosphatase (Santa Cruz Biotechnology), membranes were then treated with an Nitro blue tetrazolium chloride/5-bromo-4-chloro-3-indolyl phosphate substrate solution (Roche) for staining.

Electron Microscopy and Immunogold Labeling

Source leaves from *avp1-2* plants were processed as described previously (Paez-Valencia et al., 2011). For the immunogold labeling experiments, anti-AVP1 sera (Paez-Valencia et al., 2011) were used.

Double-Immunofluorescence Staining

Samples were prepared as described above ("AVP1 Immunolocalization"). After blocking, slides were incubated with the following primary antibodies: rabbit anti-*E. coli*-soluble ppa and mouse anti-PM ATPase (AHA3) at a dilution of 1:200 in PBS Tween or preimmune sera for 1 h at room temperature. Antigen-antibody complexes were revealed with goat anti-mouse IgG coupled to fluorescein isothiocyanate (Santa Cruz Biotechnology) for AHA3 and goat anti-rabbit coupled to Alexa 568 (Molecular Probe; Invitrogen) for *E. coli* ppa. All sections were mounted using Vectashield Mounting Media (Vector Laboratories). The fluorescence was excited with 488 nm of light (AHA3; green fluorescence) and 568 nm of light (ppa; red fluorescence).

Statistical Analysis

Statistical analysis (unless specified otherwise) was performed with Excel 2007 software (Microsoft Office). Student's *t* test was used along the different experiments to analyze the significance of differences against Col-0 (wild-type plants) in each point or treatment. The significance of the *P* values were indicated as $^{**}P \leq 0.01$, $^{*}P \leq 0.05$, and $^{\#}P \leq 0.07$ for all analyses.

Sequence data from this article can be found in the GenBank/EMBL data libraries under accession numbers *KUP2* (At2g40540), *NRT2.1* (At1g08090), *NRT2.4* (At5g60770), *PHT1.4* (At2g38940), *CLH1* (At4g24550), *GAPDH3* (AT1g13440), *AtSUC2* (AT1g22710), *AVP1* (At1g15690), *UBQ10* (At4g05320), and *avp1-2* T-DNA (SALK046492).

Supplemental Data

The following supplemental materials are available.

Supplemental Figure S1. GUS staining patterns of an *AVP1* 1.7-kb promoter-β-glucuronidase reporter in Columbia-0 seedlings and adult plants.

Supplemental Figure S2. Phloem-specific *AVP1* silencing in *AVP1-1* plants.

Supplemental Figure S3. Putative DOF2 core binding sites present in the 244-bp *AVP1* promoter sequence.

Supplemental Figure S4. Genotypic confirmation of T2 *avp1-2* lines transformed with an *E. coli*-soluble PPase driven by a phloem-specific promoter.

Supplemental Figure S5. Comparative growth phenotypes of Columbia-0 and *AVP1* mutants.

Supplemental Table S1. List of primers.

ACKNOWLEDGMENTS

We thank Masayoshi Maeshima (Nagoya University) and Ali Ferjani (Tokyo Gakugei University) for providing seeds of *vhp1-1* and *fugu5-1*, respectively, and Dr. Debra Baluch (W. M. Keck Bioimaging Facility, Arizona State University) for assistance with the use of the confocal microscope.

Received November 25, 2014; accepted February 12, 2015; published February 13, 2015.

LITERATURE CITED

Arif A, Zafar Y, Arif M, Blumwald E (2013) Improved growth, drought tolerance, and ultrastructural evidence of increased turgidity in tobacco plants overexpressing Arabidopsis vacuolar pyrophosphatase (AVP1). Mol Biotechnol **54:** 379–392

Ayre BG (2011) Membrane-transport systems for sucrose in relation to whole-plant carbon partitioning. Mol Plant **4:** 377–394

Baltscheffsky H, Von Stedingk LV, Heldt HW, Klingenberg M (1966) Inorganic pyrophosphate: formation in bacterial photophosphorylation. Science **153:** 1120–1122

Bao AK, Wang SM, Wu GQ, Xi JJ, Zhang JL, Wang CM (2009) Overexpression of the Arabidopsis H^+-PPase enhanced resistance to salt and drought stress in transgenic alfalfa (Medicago sativa L.). Plant Sci **176:** 232–240

Benfey PN, Chua NH (1990) The cauliflower mosaic virus 35S promoter: combinatorial regulation of transcription in plants. Science **250:** 959–966

Braun DM, Wang L, Ruan YL (2014) Understanding and manipulating sucrose phloem loading, unloading, metabolism, and signalling to enhance crop yield and food security. J Exp Bot **65:** 1713–1735

Clough SJ, Bent AF (1998) Floral dip: a simplified method for *Agrobacterium*-mediated transformation of *Arabidopsis thaliana*. Plant J **16:** 735–743

Curtis MD, Grossniklaus U (2003) A gateway cloning vector set for high-throughput functional analysis of genes in planta. Plant Physiol **133:** 462–469

Dasgupta K, Khadilkar AS, Sulpice R, Pant B, Scheible WR, Fisahn J, Stitt M, Ayre BG (2014) Expression of sucrose transporter cDNAs specifically in companion cells enhances phloem loading and long-distance transport of sucrose but leads to an inhibition of growth and the perception of a phosphate limitation. Plant Physiol **165:** 715–731

Davies JM (1997) The bioenergetics of vacuolar H+ pumps. *In* RA Leigh, D Sanders, eds, The Plant Vacuole, Ed 1, Vol 25. Academic Press, San Diego, pp 340–363

Desfeux C, Clough SJ, Bent AF (2000) Female reproductive tissues are the primary target of Agrobacterium-mediated transformation by the Arabidopsis floral-dip method. Plant Physiol **123:** 895–904

DeWitt ND, Harper JF, Sussman MR (1991) Evidence for a plasma membrane proton pump in phloem cells of higher plants. Plant J **1:** 121–128

Ferjani A, Segami S, Horiguchi G, Muto Y, Maeshima M, Tsukaya H (2011) Keep an eye on PPi: the vacuolar-type H+-pyrophosphatase regulates postgerminative development in *Arabidopsis*. Plant Cell **23:** 2895–2908

Gaxiola RA, Fink GR, Hirschi KD (2002) Genetic manipulation of vacuolar proton pumps and transporters. Plant Physiol **129:** 967–973

Gaxiola RA, Li J, Undurraga S, Dang LM, Allen GJ, Alper SL, Fink GR (2001) Drought- and salt-tolerant plants result from overexpression of the AVP1 H+-pump. Proc Natl Acad Sci USA **98:** 11444–11449

Gaxiola RA, Palmgren MG, Schumacher K (2007) Plant proton pumps. FEBS Lett **581:** 2204–2214

Gaxiola RA, Sanchez CA, Paez-Valencia J, Ayre BG, Elser JJ (2012) Genetic manipulation of a "vacuolar" H(+)-PPase: from salt tolerance to yield enhancement under phosphorus-deficient soils. Plant Physiol **159:** 3–11

Giaquinta RT, Lin W, Sadler NL, Franceschi VR (1983) Pathway of phloem unloading of sucrose in corn roots. Plant Physiol **72:** 362–367

Gottwald JR, Krysan PJ, Young JC, Evert RF, Sussman MR (2000) Genetic evidence for the *in planta* role of phloem-specific plasma membrane sucrose transporters. Proc Natl Acad Sci USA **97:** 13979–13984

Harrison SJ, Mott EK, Parsley K, Aspinall S, Gray JC, Cottage A (2006) A rapid and robust method of identifying transformed Arabidopsis thaliana seedlings following floral dip transformation. Plant Methods **2:** 19

Imlau A, Truernit E, Sauer N (1999) Cell-to-cell and long-distance trafficking of the green fluorescent protein in the phloem and symplastic unloading of the protein into sink tissues. Plant Cell **11:** 309–322

Jelitto T, Sonnewald U, Willmitzer L, Hajirezeai M, Stitt M (1992) Inorganic pyrophosphate content and metabolites in potato and tobacco plants expressing E. coli pyrophosphatase in their cytosol. Planta **188:** 238–244

Jha D, Shirley N, Tester M, Roy SJ (2010) Variation in salinity tolerance and shoot sodium accumulation in Arabidopsis ecotypes linked to differences in the natural expression levels of transporters involved in sodium transport. Plant Cell Environ **33:** 793–804

Kircher S, Schopfer P (2012) Photosynthetic sucrose acts as cotyledon-derived long-distance signal to control root growth during early seedling development in Arabidopsis. Proc Natl Acad Sci USA **109:** 11217–11221

Kobae Y, Uemura T, Sato MH, Ohnishi M, Mimura T, Nakagawa T, Maeshima M (2004) Zinc transporter of Arabidopsis thaliana AtMTP1 is localized to vacuolar membranes and implicated in zinc homeostasis. Plant Cell Physiol **45:** 1749–1758

Lahti R, Pitkäranta T, Valve E, Ilta I, Kukko-Kalske E, Heinonen J (1988) Cloning and characterization of the gene encoding inorganic pyrophosphatase of Escherichia coli K-12. J Bacteriol **170:** 5901–5907

Langhans M, Ratajczak R, Lützelschwab M, Michalke W, Wächter R, Fischer-Schliebs E, Ullrich CI (2001) Immunolocalization of plasmamembrane H+-ATPase and tonoplast-type pyrophosphatase in the plasma membrane of the sieve element-companion cell complex in the stem of Ricinus communis L. Planta **213:** 11–19

Le Hir R, Bellini C (2013) The plant-specific dof transcription factors family: new players involved in vascular system development and functioning in Arabidopsis. Front Plant Sci **4:** 164

Lejay L, Wirth J, Pervent M, Cross JM, Tillard P, Gojon A (2008) Oxidative pentose phosphate pathway-dependent sugar sensing as a mechanism for regulation of root ion transporters by photosynthesis. Plant Physiol **146:** 2036–2053

Lerchl J, Geigenberger P, Stitt M, Sonnewald U (1995) Impaired photoassimilate partitioning caused by phloem-specific removal of pyrophosphate can be complemented by a phloem-specific cytosolic yeast-derived invertase in transgenic plants. Plant Cell **7:** 259–270

Li B, Wei A, Song C, Li N, Zhang J (2008) Heterologous expression of the *TsVP* gene improves the drought resistance of maize. Plant Biotechnol J **6:** 146–159

Li J, Yang H, Peer WA, Richter G, Blakeslee J, Bandyopadhyay A, Titapiwantakun B, Undurraga S, Khodakovskaya M, Richards EL, et al (2005) Arabidopsis H+-PPase AVP1 regulates auxin-mediated organ development. Science **310:** 121–125

Li X, Guo C, Gu J, Duan W, Zhao M, Ma C, Du X, Lu W, Xiao K (2014) Overexpression of VP, a vacuolar H+-pyrophosphatase gene in wheat (Triticum aestivum L.), improves tobacco plant growth under Pi and N deprivation, high salinity, and drought. J Exp Bot **65:** 683–696

Long AR, Williams LE, Nelson SJ, Hall J (1995) Localization of membrane pyrophosphatase activity in *Ricinus communis* seedlings. J Plant Physiol **146:** 629–638

Lv S, Zhang K, Gao Q, Lian L, Song Y, Zhang J (2008) Overexpression of an H+-PPase gene from Thellungiella halophila in cotton enhances salt tolerance and improves growth and photosynthetic performance. Plant Cell Physiol **49:** 1150–1164

Marsh K, Gonzalez P, Echeverria E (2000) PPi formation by reversal of the tonoplast-bound H+-pyrophosphatase from 'Valencia' orange juice cells. J Am Soc Hortic Sci **125:** 420–424

Martinoia E, Maeshima M, Neuhaus HE (2007) Vacuolar transporters and their essential role in plant metabolism. J Exp Bot **58:** 83–102

Matsuda Y, Liang G, Zhu Y, Ma F, Nelson RS, Ding B (2002) The Commelina yellow mottle virus promoter drives companion-cell-specific gene expression in multiple organs of transgenic tobacco. Protoplasma **220:** 51–58

Medberry SL, Lockhart BE, Olszewski NE (1992) The Commelina yellow mottle virus promoter is a strong promoter in vascular and reproductive tissues. Plant Cell **4:** 185–192

Medberry SL, Olszewski NE (1993) Identification of cis elements involved in Commelina yellow mottle virus promoter activity. Plant J **3:** 619–626

Mitsuda N, Takeyasu K, Sato MH (2001) Pollen-specific regulation of vacuolar H+-PPase expression by multiple cis-acting elements. Plant Mol Biol **46:** 185–192

Müller LM, von Korff M, Davis SJ (2014) Connections between circadian clocks and carbon metabolism reveal species-specific effects on growth control. J Exp Bot **65:** 2915–2923

Noguero M, Atif RM, Ochatt S, Thompson RD (2013) The role of the DNA-binding One Zinc Finger (DOF) transcription factor family in plants. Plant Sci **209:** 32–45

Paez-Valencia J, Patron-Soberano A, Rodriguez-Leviz A, Sanchez-Lares J, Sanchez-Gomez C, Valencia-Mayoral P, Diaz-Rosas G, Gaxiola R

(2011) Plasma membrane localization of the type I H(+)-PPase AVP1 in sieve element-companion cell complexes from Arabidopsis thaliana. Plant Sci **181:** 23–30

Paez-Valencia J, Sanchez-Lares J, Marsh E, Dorneles LT, Santos MP, Sanchez D, Winter A, Murphy S, Cox J, Trzaska M, et al (2013) Enhanced proton translocating pyrophosphatase activity improves nitrogen use efficiency in romaine lettuce. Plant Physiol **161:** 1557–1569

Park S, Li J, Pittman JK, Berkowitz GA, Yang H, Undurraga S, Morris J, Hirschi KD, Gaxiola RA (2005) Up-regulation of a H^+-pyrophosphatase (H^+-PPase) as a strategy to engineer drought-resistant crop plants. Proc Natl Acad Sci USA **102:** 18830–18835

Pasapula V, Shen G, Kuppu S, Paez-Valencia J, Mendoza M, Hou P, Chen J, Qiu X, Zhu L, Zhang X, et al (2011) Expression of an Arabidopsis vacuolar H+-pyrophosphatase gene (AVP1) in cotton improves drought- and salt tolerance and increases fibre yield in the field conditions. Plant Biotechnol J **9:** 88–99

Pei L, Wang J, Li K, Li Y, Li B, Gao F, Yang A (2012) Overexpression of Thellungiella halophila H+-pyrophosphatase gene improves low phosphate tolerance in maize. PLoS ONE **7:** e43501

Ratajczak R, Hinz G, Robinson DG (1999) Localization of pyrophosphatase in membranes of cauliflower inflorescence cells. Planta **208:** 205–211

Rea PA, Kim Y, Sarafian V, Poole RJ, Davies JM, Sanders D (1992) Vacuolar H(+)-translocating pyrophosphatases: a new category of ion translocase. Trends Biochem Sci **17:** 348–353

Rennie EA, Turgeon R (2009) A comprehensive picture of phloem loading strategies. Proc Natl Acad Sci USA **106:** 14162–14167

Rocha Facanha A, de Meis L (1998) Reversibility of H^+-ATPase and H^+-pyrophosphatase in tonoplast vesicles from maize coleoptiles and seeds. Plant Physiol **116:** 1487–1495

Ruan YL (2014) Sucrose metabolism: gateway to diverse carbon use and sugar signaling. Annu Rev Plant Biol **65:** 33–67

Schilling RK, Marschner P, Shavrukov Y, Berger B, Tester M, Roy SJ, Plett DC (2014) Expression of the Arabidopsis vacuolar H^+-pyrophosphatase gene (AVP1) improves the shoot biomass of transgenic barley and increases grain yield in a saline field. Plant Biotechnol J **12:** 378–386

Schneidereit A, Imlau A, Sauer N (2008) Conserved cis-regulatory elements for DNA-binding-with-one-finger and homeo-domain-leucine-zipper transcription factors regulate companion cell-specific expression of the Arabidopsis thaliana SUCROSE TRANSPORTER 2 gene. Planta **228:** 651–662

Schumaker KS, Sze H (1985) A Ca/H antiport system driven by the proton electrochemical gradient of a tonoplast H-ATPase from oat roots. Plant Physiol **79:** 1111–1117

Segami S, Makino S, Miyake A, Asaoka M, Maeshima M (2014) Dynamics of vacuoles and H+-pyrophosphatase visualized by monomeric green fluorescent protein in *Arabidopsis*: artifactual bulbs and native intravacuolar spherical structures. Plant Cell **26:** 3416–3434

Seufferheld M, Lea CR, Vieira M, Oldfield E, Docampo R (2004) The H(+)-pyrophosphatase of *Rhodospirillum rubrum* is predominantly located in polyphosphate-rich acidocalcisomes. J Biol Chem **279:** 51193–51202

Seufferheld MJ, Kim KM, Whitfield J, Valerio A, Caetano-Anollés G (2011) Evolution of vacuolar proton pyrophosphatase domains and volutin granules: clues into the early evolutionary origin of the acidocalcisome. Biol Direct **6:** 50

Sonnewald U (1992) Expression of E. coli inorganic pyrophosphatase in transgenic plants alters photoassimilate partitioning. Plant J **2:** 571–581

Srivastava AC, Ganesan S, Ismail IO, Ayre BG (2008) Functional characterization of the Arabidopsis AtSUC2 Sucrose/H+ symporter by tissue-specific complementation reveals an essential role in phloem loading but not in long-distance transport. Plant Physiol **148:** 200–211

Sulpice R, Pyl ET, Ishihara H, Trenkamp S, Steinfath M, Witucka-Wall H, Gibon Y, Usadel B, Poree F, Piques MC, et al (2009) Starch as a major integrator in the regulation of plant growth. Proc Natl Acad Sci USA **106:** 10348–10353

Thole V, Worland B, Snape JW, Vain P (2007) The pCLEAN dual binary vector system for Agrobacterium-mediated plant transformation. Plant Physiol **145:** 1211–1219

Töpfer R, Matzeit V, Gronenborn B, Schell J, Steinbiss HH (1987) A set of plant expression vectors for transcriptional and translational fusions. Nucleic Acids Res **15:** 5890

Truernit E, Sauer N (1995) The promoter of the Arabidopsis thaliana SUC2 sucrose-H+ symporter gene directs expression of beta-glucuronidase to the phloem: evidence for phloem loading and unloading by SUC2. Planta **196:** 564–570

Turgeon R, Webb JA (1973) Leaf development and phloem transport in Cucurbita pepo: transition from import to export. Planta **113:** 179–191

Undurraga SF, Santos MP, Paez-Valencia J, Yang H, Hepler PK, Facanha AR, Hirschi KD, Gaxiola RA (2012) Arabidopsis sodium dependent and independent phenotypes triggered by H^+-PPase up-regulation are SOS1 dependent. Plant Sci **183:** 96–105

Wang JW, Wang HQ, Xiang WW, Chai TY (2014) A Medicago truncatula H+-pyrophosphatase gene, MtVP1, improves sucrose accumulation and anthocyanin biosynthesis in potato (Solanum tuberosum L.). Genet Mol Res **13:** 3615–3626

Ward JM, Kühn C, Tegeder M, Frommer WB (1998) Sucrose transport in higher plants. Int Rev Cytol **178:** 41–71

Wright KM, Roberts AG, Martens HJ, Sauer N, Oparka KJ (2003) Structural and functional vein maturation in developing tobacco leaves in relation to *AtSUC2* promoter activity. Plant Physiol **131:** 1555–1565

Yang H, Knapp J, Koirala P, Rajagopal D, Peer WA, Silbart LK, Murphy A, Gaxiola RA (2007) Enhanced phosphorus nutrition in monocots and dicots over-expressing a phosphorus-responsive type I H+-pyrophosphatase. Plant Biotechnol J **5:** 735–745

Yang H, Zhang X, Gaxiola RA, Xu G, Peer WA, Murphy AS (2014) Overexpression of the Arabidopsis proton-pyrophosphatase AVP1 enhances transplant survival, root mass, and fruit development under limiting phosphorus conditions. J Exp Bot **65:** 3045–3053

Yazdanbakhsh N, Sulpice R, Graf A, Stitt M, Fisahn J (2011) Circadian control of root elongation and C partitioning in Arabidopsis thaliana. Plant Cell Environ **34:** 877–894

Zhao C, Craig JC, Petzold HE, Dickerman AW, Beers EP (2005) The xylem and phloem transcriptomes from secondary tissues of the Arabidopsis root-hypocotyl. Plant Physiol **138:** 803–818